

Spin-current driven Dzyaloshinskii-Moriya interaction in multiferroic BiFeO<sub>3</sub> from first principlesSebastian Meyer<sup>1</sup>, Bin Xu<sup>2,3</sup>, Matthieu J. Verstraete<sup>1</sup>, Laurent Bellaiche<sup>3</sup>, and Bertrand Dupé<sup>1,4</sup><sup>1</sup>Nanomaterials/Quantum Materials/CESAM, Université de Liège, B-4000 Sart Tilman, Belgium<sup>2</sup>Jiangsu Key Laboratory of Thin Films, School of Physical Science and Technology, Soochow University, Suzhou 215006, China<sup>3</sup>Physics Department and Institute for Nanoscience and Engineering, University of Arkansas, Fayetteville, Arkansas 72701, USA<sup>4</sup>Fonds de la Recherche Scientifique (FRS-FNRS), B-1000 Bruxelles, Belgium

(Received 5 September 2022; revised 11 April 2023; accepted 9 June 2023; published 5 July 2023)

The electrical control of magnons opens up new ways to transport and process information for logic devices. In magnetoelectrical multiferroics, the Dzyaloshinskii-Moriya (DM) interaction directly allows for such control and hence is of major importance. We determine the origin and the strength of the (converse) spin-current DM interaction in the *R3c* bulk phase of multiferroic BiFeO<sub>3</sub> based on density functional theory. Our data support only the existence of one DM interaction contribution originating from the spin-current model. By exploring the magnon dispersion in the full Brillouin zone, we show that the exchange is isotropic, but the DM interaction and anisotropy prefer any propagation and any magnetization direction within the full (111) plane. Our work emphasizes the significance of the asymmetric potential induced by the spin current over the structural asymmetry induced by the anionic octahedron in multiferroics such as BiFeO<sub>3</sub>.

DOI: [10.1103/PhysRevB.108.024403](https://doi.org/10.1103/PhysRevB.108.024403)

## I. INTRODUCTION

BiFeO<sub>3</sub> (BFO) is one of the few single-phase multiferroics which exhibit a large spontaneous polarization and a long-range magnetic order at room temperature. BFO has an antiferromagnetic (AFM) texture that can be approximated locally by a G-type order in its *R3c* ground state with a Néel temperature of 643 K [1]. *R3c* BFO exhibits a polarization of about 90  $\mu\text{C}/\text{cm}^2$  along the pseudocubic  $\langle 111 \rangle$  symmetry equivalent directions with a Curie temperature of 1123 K [2–5]. In bulk, the AFM order is modified by the Dzyaloshinskii-Moriya (DM) interaction [6,7] creating a spin spiral that propagates along the  $[1\bar{1}0]$  direction (known as the type-I cycloid), with magnetic moments lying in the plane formed by the polarization and the propagation direction. The periodicity of this spin spiral is 62 nm [8,9]. Additionally, another propagation direction along  $[11\bar{2}]$  has been reported in BFO, and is referred to as the type-II cycloid [10–14].

The AFM spin spiral couples to the polarization via the magnetoelectric (ME) effect. The ME effect can have multiple origins [15]. Some are indirect, such as magnetostriction [16] or spin-dependent screening [17], while others, such as the DM interaction, directly couple the atomic displacements to the AFM spin spiral, opening up the possibility of the electrical control of magnons [18]. This effect is at the center of a new logic device which is intended to electrically control out-of-equilibrium spin spirals—also called magnons—in BFO to transport and process information [19,20]. Therefore exploration of the stability mechanisms of different types of spin spirals is of paramount importance and has been the subject of a lot of research.

A phenomenological model based on Lifshitz invariants established that the DM interaction stabilizing the spin spiral had the form  $\alpha(P) \cdot \mathbf{L}_i \times \mathbf{L}_j$ , where  $P$  is the polarization and

$\mathbf{L}$  is the AFM vector [21]. This phenomenological model was completed by a microscopic model based on the tight-binding approximation which attributed the presence of a nonzero polarization to the presence of a spin spiral. In this model, the hybridization between the *d* orbitals of the metal ions and the *p* orbitals of the oxygen results in the polarization  $\mathbf{P} \propto \mathbf{e}_{ij} \times (\mathbf{S}_i \times \mathbf{S}_j)$ , where  $\mathbf{S}_i$  and  $\mathbf{S}_j$  are spins on sites *i* and *j*, respectively, and  $\mathbf{e}_{ij}$  is the unit vector between sites *i* and *j* [22].

The link between this polarization and the presence of the DM interaction was explicitly written by Rahmedov *et al.* in Ref. [23], where the spin spiral in BFO was explained based on the presence of two chiral interactions of different symmetries. The first term,  $\mathbf{D}_{\text{wFM}} \propto (\boldsymbol{\omega}_i - \boldsymbol{\omega}_j) \cdot (\mathbf{S}_i \times \mathbf{S}_j)$ , couples the oxygen octahedra tilts  $\boldsymbol{\omega}$  to the magnetic texture and stabilizes the magnetic moment in the (111) plane perpendicular to the tilts' rotation vectors. This DM contribution induces the weak ferromagnetic moment in BFO [24]. The second term has the form  $\mathbf{D}_{\text{SC}} \propto (\mathbf{u}_i \times \mathbf{e}_{ij}) \cdot (\mathbf{S}_i \times \mathbf{S}_j)$ , couples the polarization direction  $\mathbf{u}_i$  to the magnetic moments, and favors the stabilization of the magnetic moments perpendicular to the (111) plane. By varying these energy terms, several types of spin cycloids have been predicted in BFO [25].

To compare the energies of these different spin spirals, both DM contributions must be computed from density functional theory (DFT).  $\mathbf{D}_{\text{wFM}}$  was predicted to create the weak magnetic moment in BFO, and therefore it should lie along the  $[111]$  direction [24]. This DM contribution was obtained from DFT calculations (from 146  $\mu\text{eV}$  [26] up to 304  $\mu\text{eV}$  [27]) in relatively good agreement with the experimental value (163  $\mu\text{eV}$  [28]). Note that a full parametrization of BFO in the *R3c* phase obtained from experimental measurements is given in Refs. [29–31]. They found  $\mathbf{D}_{\text{SC}} = 110 \mu\text{eV}$  and  $\mathbf{D}_{\text{wFM}} = 50 \mu\text{eV}$ , which values are significantly lower than previous measurements and calculations. However, to our surprise and

to the best of our knowledge,  $\mathbf{D}_{\text{SC}}$  has not been obtained from DFT calculations, which does not allow us to discuss the stability of the different spin spirals.

Here, we determine the origin and the strength of the spin-current DM interaction in  $\text{BiFeO}_3$  from DFT and show that in this type of multiferroic, the DM interaction originates from the asymmetric potential within the Fe cations rather than the structural distortions induced by the O anionic octahedra. We calculate the energies of spin spirals  $E(\mathbf{q})$  for different propagation directions  $\mathbf{q}$  in the full pseudocubic Brillouin zone (BZ), which shows an isotropic exchange interaction. The spin-orbit coupling (SOC) contribution is fully quenched for spin spirals propagating along the polarization direction, which only agrees with the spin-current model [22,23] and excludes the model of Fert and Levy [32] (referred to herein as the Levy-Fert model (LF model)). Finally, all magnetic interactions, e.g., the magnetic exchange, the spin-current model, and the anisotropy, lead to a degeneracy of spin cycloids within the (111) plane which suggests that both type-I and type-II cycloids could coexist in bulk  $R3c$  BFO.

## II. METHODS

We have used the relaxed structure of bulk  $\text{BiFeO}_3$  and calculated the energy dispersions  $E(\mathbf{q})$  of flat spin spiral states without and with spin-orbit coupling to determine the magnetic exchange interaction and Dzyaloshinskii-Moriya interaction. The details are as follows.

### A. Structure of $\text{BiFeO}_3$

We used the  $R3c$  structure of  $\text{BiFeO}_3$  from Ref. [33], where the unit cell of BFO contains ten atoms and has been relaxed with DFT using the ABINIT package [34–36] and the projector augmented wave (PAW) method [37]. The exchange and correlation functional is treated with the local spin density approximation +  $U$  (LSDA+ $U$ ), with a Hubbard  $U$  parameter of 4.0 eV and  $J$  of 0.4 eV on the Fe atoms. The wave functions have been expanded using plane-wave basis sets with a kinetic energy cutoff of 30 hartrees. The self-consistent calculations have been performed with an unshifted  $24 \times 24 \times 24$   $k$ -point grid. For the structural relaxation, the collinear G-type AFM configuration has been adopted. The  $R3c$  structure was optimized until the force on each atom was smaller than  $1 \times 10^{-5}$  hartrees/bohr. The relaxed rhombohedral lattice constant of BFO is 5.538 Å, and the rhombohedral angle is  $59.71^\circ$ .

### B. Energy dispersion of spin spirals

We use the abovementioned structure and calculate the energy dispersion  $E(\mathbf{q})$  of flat homogeneous spin spirals applying the full-potential linearized augmented plane wave (FLAPW) approach [38–40], as implemented in the FLEUR code [41]. For all these calculations, we have used the LSDA+ $U$  [42], muffin-tin radii of 2.80, 2.29, and 1.29 bohrs for Bi, Fe, and O atoms, respectively and a large plane-wave cutoff  $k_{\text{max}}$  of 4.6 bohr $^{-1}$ . These parameters result in a magnetic moment of  $m = 4 \mu_{\text{B}}$  in agreement with experiments [9]. Spin spirals are the general solution of the Heisenberg model on a periodic lattice and can be characterized by the spin spiral

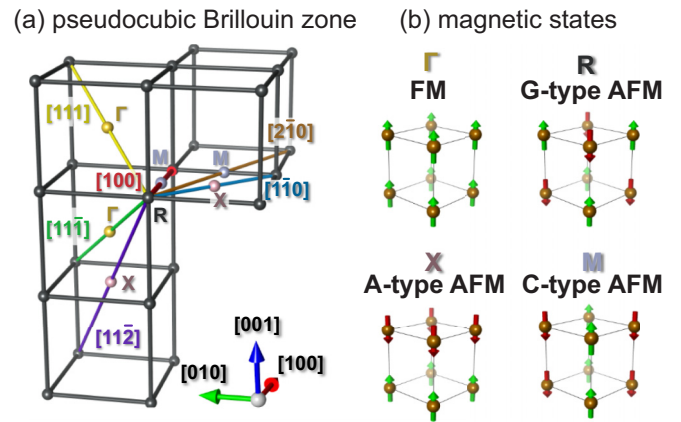


FIG. 1. (a) Pseudocubic Brillouin zone (BZ) with high-symmetry points (red points and letters). Shown are the calculated propagation directions (colored lines) of spin spirals. Note that all calculations start from the same  $R$  point. (b) Collinear magnetic states (FM, ferromagnetic; AFM, antiferromagnetic) connected to each high-symmetry point of the BZ.

vector  $\mathbf{q}$ . This vector determines the propagation direction of the spin spiral as well as the canting angle between two neighboring spins. A magnetic moment  $\mathbf{S}_i$  at an atom position  $\mathbf{r}_i$  is given by

$$\mathbf{S}_i = S(\cos(\mathbf{q} \cdot \mathbf{r}_i), \sin(\mathbf{q} \cdot \mathbf{r}_i), 0), \quad (1)$$

where  $S$  is the magnitude of the magnetic moment. The vector  $\mathbf{q}$  is a vector in reciprocal space, and we apply it along several high-symmetry directions of the rhombohedral BZ. For simplification, we present all data within the pseudocubic Brillouin zone, shown in Fig. 1(a). The different directions are drawn as colored lines, starting from the  $R$  point. Every high-symmetry point in the BZ is connected to a certain collinear state, sketched in Fig. 1(b). The starting point of every direction is the  $R$  point with the coordinates  $\mathbf{q} = (1/2, 1/2, 1/2) \frac{2\pi}{a}$  of the pseudocubic BZ. For convenient illustration in our data, all paths are connected with their common high-symmetry points. The calculations along the full paths without SOC have been performed self-consistently using the generalized Bloch theorem [43] and a  $k$ -point mesh of  $10 \times 10 \times 10$ . To accurately determine the energies around the magnetic ground state ( $R$  points) at  $|\mathbf{q}| \rightarrow R$ , the magnetic force theorem [44,45] has been applied using a dense  $k$ -point set of 8000  $k$  points (i.e.,  $20 \times 20 \times 20$ ). The energy dispersion without SOC is interpreted using the Heisenberg exchange interaction (see paragraph on exchange interaction in Sec. II C). For the energy contribution due to SOC ( $\Delta E_{\text{SOC}}$ ) in spin spirals, we add SOC in first-order perturbation theory [46] for every previously calculated point. The resulting curve has been interpreted with the Dzyaloshinskii-Moriya interaction. Note that we applied SOC perpendicular to  $\mathbf{q}$  in several directions: Shown is the maximum contribution of each direction.

### C. Magnetic interactions

We interpret our DFT calculations using a magnetic Hamiltonian containing the symmetric exchange interaction, the antisymmetric Dzyaloshinskii-Moriya interaction, and the

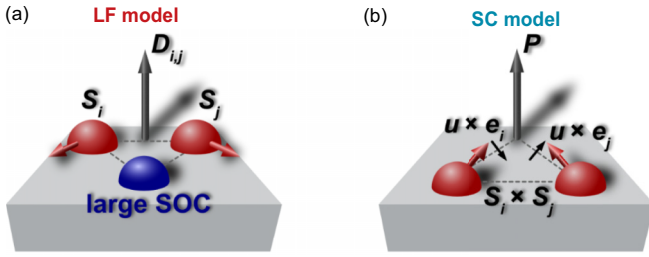


FIG. 2. Sketches of the two models for the Dzyaloshinskii-Moriya (DM) interaction used in this paper. (a) Levy-Fert model (LF model) [32,49]: Two magnetic atoms  $\mathbf{S}_i, \mathbf{S}_j$  are interacting via a heavy metal atom hosting large spin-orbit coupling (SOC). The triangle formed by the three atoms defines the DM vector  $\mathbf{D}_{ij}$ . (b) Converse spin-current (SC) model [22,23]: In systems with a polarization  $\mathbf{P}$ , the spin-current vector  $\mathbf{u} \times \mathbf{e}_{i,j}$  is perpendicular to the direction of polarization.

uniaxial or single-ion anisotropy energy. Due to our method, we are able to separately determine the different magnetic interactions.

*Exchange interaction.* The Heisenberg exchange interaction constants  $J_{ij}$  beyond nearest neighbors are determined by mapping the Heisenberg Hamiltonian

$$\mathcal{H}_{\text{ex}} = - \sum_{ij} J_{ij} (\mathbf{S}_i \cdot \mathbf{S}_j) \quad (2)$$

onto the resulting energy dispersion  $E(\mathbf{q})$  without SOC. For the fitting procedure, we have included seven neighbors ( $J_1, \dots, J_7$ ).

*Dzyaloshinskii-Moriya interaction.* To determine the Dzyaloshinskii-Moriya (DM) interaction, we analyze the energy contribution due to SOC ( $\Delta E_{\text{SOC}}$ ) of the spin spiral states which have been calculated in the previous step without SOC. In the past when the DM interaction in BFO has been evaluated using first principles, the DM vector  $\mathbf{D}_{ij}$  between two magnetic atoms at positions  $i, j$  has been computed by considering the different Fe-O-Fe bonds [26,47], hence the Levy-Fert model (LF model) [32]. The LF model is typically explained as a superexchange mechanism between two magnetic atoms  $\mathbf{S}_i, \mathbf{S}_j$  via a third nonmagnetic atom that holds a large spin-orbit coupling [see Fig. 2(a)]. Due to the direction-dependent scattering of the electrons, noncollinear magnetic structures with a specific sense of rotation (clockwise or counterclockwise) are preferred. The symmetry of the DM vector is  $\mathbf{D}_{ij} \propto \frac{\mathbf{R}_i \times \mathbf{R}_j}{|\mathbf{R}_i \times \mathbf{R}_j|}$ , where  $\mathbf{R}_{i,j}$  are the position vectors of magnetic moments  $\mathbf{S}_{i,j}$  with respect to the atom of large SOC. In BFO, the atom of large SOC is replaced by the oxygen to form the same triangle. As in previous studies [33,47], we evaluate the strength of the DM interaction using the LF model

$$\mathcal{H}_{\text{DMI}}^{\text{LF}} = - \sum_{ij} \mathbf{D}_{ij} (\mathbf{S}_i \times \mathbf{S}_j). \quad (3)$$

Depending on the propagation direction of the spin spiral, the Levy-Fert model gives reliable results; however, as shown in this paper, it cannot capture all effects.

Hence we apply a different model to explain the energy contribution due to SOC, the so-called (converse) spin-current

model [23,48]. This model is also known as the Katsura-Nagaoka-Balatsky (KNB) model [22] and shows that a spin current  $\mathbf{j}_s \propto \mathbf{S}_i \times \mathbf{S}_j$  in a noncollinear magnet creates an electric polarization  $\mathbf{P} \propto \mathbf{e}_{ij} \times \mathbf{j}_s$ . We follow the convention of Ref. [23], where the Hamiltonian is written as

$$\mathcal{H}_{\text{DMI}}^{\text{SC}} = - \sum_{ij} C_{ij} (\mathbf{u} \times \mathbf{e}_{ij}) \cdot (\mathbf{S}_i \times \mathbf{S}_j), \quad (4)$$

where  $\mathbf{u}$  is the unit vector in the direction of polarization and  $\mathbf{e}_{ij}$  is the unit vector connecting magnetic moments  $\mathbf{S}_{i,j}$  at sites  $i, j$ . The parameter  $C_{ij}$  describes the strength of the DM interaction. The difference between the DM vector  $\mathbf{D}_{ij}$  and the SC vector  $C_{ij} (\mathbf{u} \times \mathbf{e}_{ij})$  lies within the symmetry. Depending on the symmetry of the system, however, both vectors can coincide, e.g., in two-dimensional interfaces.

*Magnetocrystalline anisotropy.* We have calculated the uniaxial magnetic anisotropy in BiFeO<sub>3</sub> within the (111) plane. For that, we have assumed the collinear G-type AFM state where we have applied SOC in the presented directions of the lattice. We applied two  $k$ -point sets ( $10 \times 10 \times 10$  and  $20 \times 20 \times 20$ ) in the whole Brillouin zone and compared self-consistent calculations (SC-DFT) with calculations applying second quantization and the force theorem (FT-DFT) [44]. The other calculational parameters are consistent with the methods above. The Hamiltonian of the magnetocrystalline anisotropy is

$$\mathcal{H}_{\text{MAE}} = - \sum_i K (\mathbf{S}_i^{[111]})^2 \quad (5)$$

with  $K$  being the energy of the uniaxial anisotropy with respect to the hard [111] axis.

### III. RESULTS

#### A. Exchange interaction

The calculated energy dispersion (shown as points) obtained without SOC is presented in Fig. 3(a), where the paths are  $R \rightarrow X \rightarrow R \rightarrow M \rightarrow R \rightarrow \Gamma \rightarrow R$  (cf. lower  $x$  axis). On the upper  $x$  axis, the respective directions according to Fig. 1 can be seen. Without SOC, the dispersion shows an energy minimum at the  $R$  point (G-type AFM state) [50] and the highest energy at the  $\Gamma$  point (the FM state). The energy dispersion is mapped onto an extended Heisenberg model, Eq. (2), to determine the strength of the Heisenberg exchange interaction parameters  $J_{ij}$  [curves in Figs. 3(a) and 3(b)] beyond nearest neighbors (see Sec. II for more information). The exchange between nearest neighbors is dominant,  $J_1 \sim -27$  meV/Fe atom, capturing the large energy differences between the high-symmetry points, but seven neighbors are necessary to describe the curvature around the  $R$  points (values can be found in Table I). A close-up around every  $R$  point is shown in Fig. 3(b). The fit to the exchange interaction results in a good description of the DFT calculations. Note that the energy differences are very small, and a numerical error on this energy scale is expected. Nevertheless, all the energies (data and fit) around the collinear state at the  $R$  points have the same curvature, e.g., the same effective exchange interaction [51]. Hence the exchange in BFO is fully isotropic

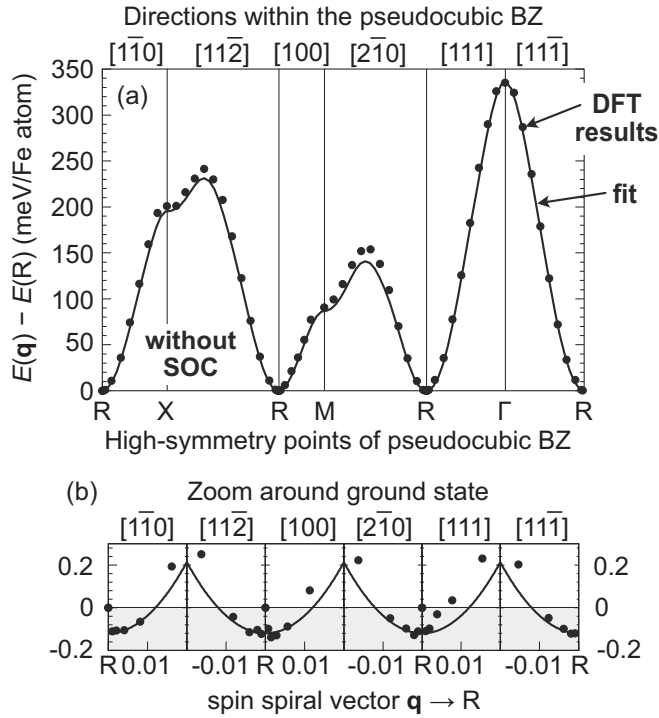


FIG. 3. Energy dispersion  $E(\mathbf{q})$  without SOC of flat spin spirals along different directions within the pseudocubic Brillouin zone. Points show calculated energies from DFT, and curves represent a fit to the Heisenberg exchange interaction including seven neighbors. (a) Full energy dispersion. (b) Zoom around the ground state at  $\mathbf{q} \rightarrow R$ .

within the pseudocubic Brillouin zone, and every direction of spin spiral is equivalent.

### B. Computing the Dzyaloshinskii-Moriya interaction

To determine the strength of the Dzyaloshinskii-Moriya (DM) interaction, we apply spin-orbit coupling (SOC) in first-order perturbation [46,52] to every calculated point of Fig. 3. The resulting energy contribution due to SOC,  $\Delta E_{\text{SOC}}$ , is illustrated in Fig. 4. While in some directions with higher symmetry [Fig. 4(a)], such as  $[1\bar{1}0]$ ,  $[100]$ , and  $[11\bar{1}]$ , the DFT results (black points) show a simple sine behavior, other directions ( $[11\bar{2}]$  and  $[2\bar{1}0]$ ) exhibit a more complex trend. In the  $[111]$  direction (the direction of spontaneous polarization in  $\text{BiFeO}_3$ ), however, the energy of SOC is completely quenched.

We quantify the strength of the DM interaction by applying the Levy-Fert model [LF model, Eq. (3)] [32] [cf. Fig. 2(a)]. In previous investigations [26,33,47], the LF model was used to describe the DM interaction in BFO, based on the DM vector  $\mathbf{D}_{ij}$  for the Fe-O-Fe bonds. We apply the fit of the LF model [red curve in Fig. 4(a)] to the DFT data. In the directions of higher symmetry, it is possible to use this model; the curve follows the correct trend of the data. However, since our calculations include specifically the  $[111]$  direction, a combined mapping of the DM vector to our data is not reproducing the DFT calculations. Hence the Levy-Fert model cannot be used to describe this kind of DM interaction in

TABLE I. Magnetic interactions in  $\text{BiFeO}_3$  mapping an atomistic spin model to the results of DFT calculations. All values of the  $i$ th-neighbor exchange  $J_i$ , the Dzyaloshinskii-Moriya constant of the spin-current model  $C_{ij}$ , and the uniaxial magnetocrystalline anisotropy  $K$  are given in the conventions “per atom” and “per pair per  $\text{m}^2$ .”  $J > 0$  ( $J < 0$ ) represents FM (AFM) order;  $C > 0$  ( $C < 0$ ) represents counterclockwise (clockwise) rotation. The effective nearest-neighbor DM term,  $C_{\text{eff}}$ , denotes a fit within the linear region of  $\Delta E_{\text{SOC}}(\mathbf{q} \rightarrow R)$ .  $K > 0$  prefers an easy plane perpendicular to the  $[111]$  direction.

Parameter	Value (meV/Fe atom)	Value (meV)
$J_1$	-26.998	-3.375
$J_2$	-2.005	-0.251
$J_3$	-0.179	-0.0224
$J_4$	+0.717	+0.0896
$J_5$	-0.195	-0.0244
$J_6$	+0.157	+0.0196
$J_7$	-0.410	-0.0513
$C_1$	+0.369	+0.0461
$C_2$	-0.00360	-0.00045
$C_3$	-0.0156	-0.00195
$C_{\text{eff}}$	+0.301	+0.00377
$K$	+0.054	+0.0068

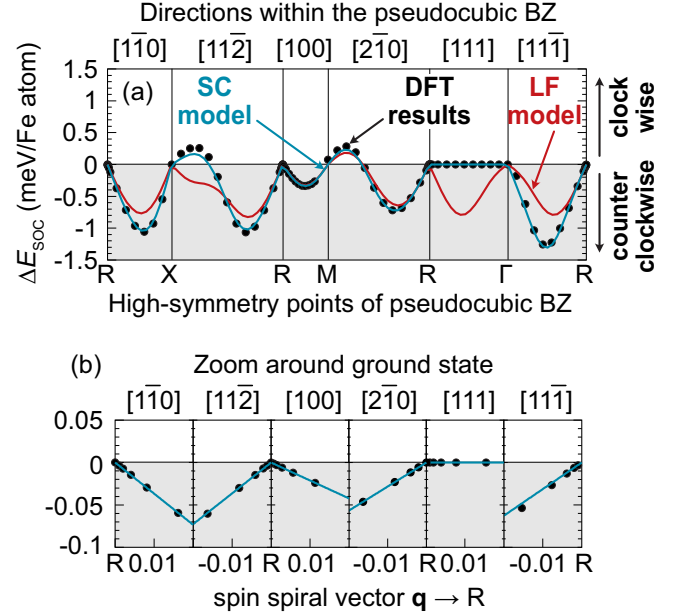


FIG. 4. Dzyaloshinskii-Moriya interaction (DM interaction) in  $\text{BiFeO}_3$ . (a) Energy contribution due to spin-orbit coupling ( $\Delta E_{\text{SOC}}$ ) to the energy dispersion of spin spirals along different directions within the pseudocubic Brillouin zone [Fig. 1(a)]. Points show calculated energies from density functional theory (DFT), the red curve corresponds to the LF model, and the blue curve corresponds to the SC model. Positive (negative) values prefer a clockwise (counterclockwise) sense of rotation of noncollinear states. (b) Zoom around the ground state at  $\mathbf{q} \rightarrow R$  where only the DFT data and the SC model are presented.

BFO. It would give rise to an energy contribution of SOC in the  $[111]$  direction. All our tests reveal completely vanishing energies in the direction of polarization.

We consider the converse spin-current model to fit the DFT data [13,22,23,25]. Mapping Eq. (4) to the energy contribution  $\Delta E_{\text{SOC}}$  gives rise to the blue curves in Figs. 4(a) and 4(b). The SC model describes the DFT results almost perfectly. Here, the fit contains three neighbors,  $C_1$ ,  $C_2$ , and  $C_3$ , where the contributions of the second and third neighbors are a minor correction to the first neighbor (cf. Table I). Note that even an effective nearest-neighbor approximation for  $C_{ij}$  (cf.  $C_{\text{eff}}$ ), a linear fit in the region of  $\Delta E_{\text{SOC}}(\mathbf{q} \rightarrow R)$ , shows a qualitatively very good agreement with the DFT calculations (see Appendix).

In Fig. 4(b), we see the energy differences between the different pseudocubic propagation directions of spin spirals around the ground state. Both the data and the SC model exhibit the steepest slope in the  $[1\bar{1}0]$  and  $[11\bar{2}]$  directions, meaning that the DM interaction for these two directions is the largest. Furthermore, for both directions, points and curves show complete energy degeneracy.  $[1\bar{1}0]$  and  $[11\bar{2}]$ , referring typically to the type-I and type-II cycloids, respectively, lie within the (111) plane. Our tests reveal that any direction within the (111) plane is equally preferred by the spin-current DM interaction. This means that including exchange and spin-current DM interaction restricts the possibility of spin cycloid propagation directions in BiFeO<sub>3</sub> bulk to any direction of the two-dimensional (111) plane. This is in accordance with Ref. [31], where it is also stated that  $\mathbf{q}$  can point along any direction in the hexagonal (111) plane considering the two magnetic interactions.

For detailed insight into the origin of the DM interaction in BFO, we calculated the element-resolved energy contribution due to SOC (Fig. 5). Here, the gray points show the total energy contribution from Fig. 4(a), and the colored points represent the elements of BiFeO<sub>3</sub> (curves serve as guides to the eye). In Figs. 5(b), 5(c), and 5(d) the energy contributions due to Bi, Fe, and O, respectively, are presented. Since, in the rhombohedral unit cell, two Bi, two Fe, and six O atoms are used, a sketch of BiFeO<sub>3</sub> in cubic representation is shown in Fig. 5(a) with the same color code for each element as in the graphs. Even though Bi is the element of large SOC and the O atoms break the inversion symmetry, their contribution to the total DM interaction in BFO is negligible [Figs. 5(b) and 5(d)]. This emphasizes that the Levy-Fert model relying on a heavy metallic element with large SOC and structural asymmetry does not provide a good description for BFO. The total DM interaction—as a sum of all contributions—is represented by the whole contribution of both Fe atoms. This is similar to the Rashba DM interaction observed in  $3d$  unsupported monolayers (UMLs) under an external electric field [53] and in graphene/Co(0001) due to the potential gradient between graphene and Co [54]. It creates an internal asymmetry of the potential leading to a nonvanishing DM interaction even though the structure itself does not hold an asymmetry. In BFO, the internal electric field creates the same asymmetry within the potential of the Fe atoms, and hence the DM interaction is driven by the spin current of the noncollinear magnetic structure.

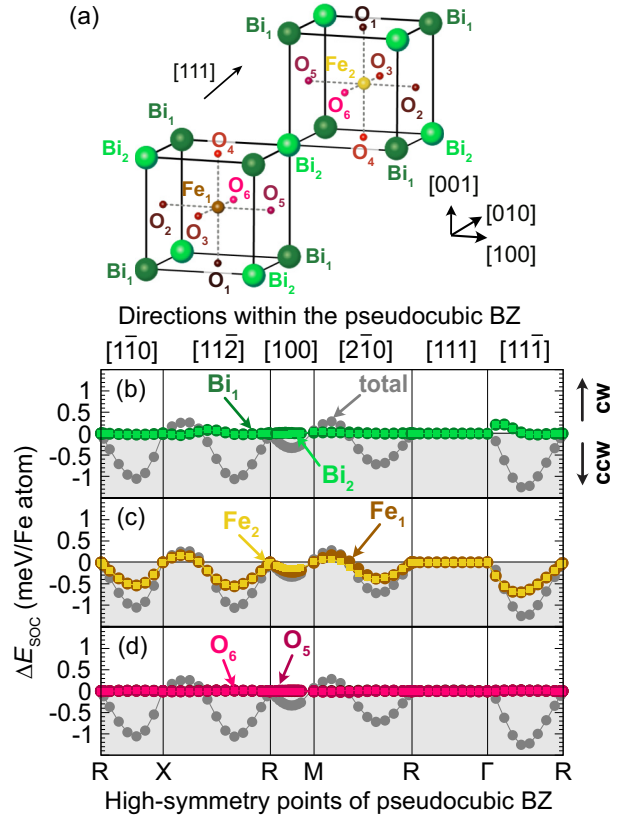


FIG. 5. Element-resolved energy contribution due to SOC ( $\Delta E_{\text{SOC}}$ ) to the energy dispersion. (a) Sketch of the BiFeO<sub>3</sub> structure in the cubic approximation. (b), (c), and (d)  $\Delta E_{\text{SOC}}$  for two Bi, two Fe, and six O atoms in the unit cell, respectively. The total energy contribution is shown with gray points. Here, cw, clockwise; ccw, counterclockwise.

### C. Magnetocrystalline anisotropy

As mentioned above, the exchange is isotropic within the full three-dimensional (3D) BZ, whereas the spin-current driven DM interaction narrows the spin cycloid directions down to the (111) plane. However, experiments on bulk  $R3c$  BFO only observed type-I cycloids, propagating in  $[1\bar{1}0]$  and the two equivalent directions  $[\bar{1}01]$  and  $[01\bar{1}]$ . Therefore we determine the uniaxial anisotropy energy to check whether this interaction can pin the cycloid's propagation down to these three directions. In Ref. [33] it has been shown that the small easy-plane (111) anisotropy in  $R3c$  BFO is a result of both strong out-of-plane anisotropy (in the  $[111]$  direction) driven by the Bi-Fe ferroelectric displacement in competition with a strong easy-plane anisotropy (perpendicular to the  $[111]$  direction) stemming from the oxygen octahedra tilts. Here, we calculate the anisotropy energy using a  $360^\circ$  rotation within the (111) plane [cf. arrows in the (111) plane of Fig. 6(a)]. The magnetocrystalline anisotropy energy (MAE) is not changing for any direction in this plane, which is shown in Fig. 6(b). In bulk BFO, the MAE does not prefer a certain magnetization direction within the (111) plane. Note that this is in accordance with Ref. [31], where the degeneracy between type-I and type-II spin cycloids is lifted by introducing an

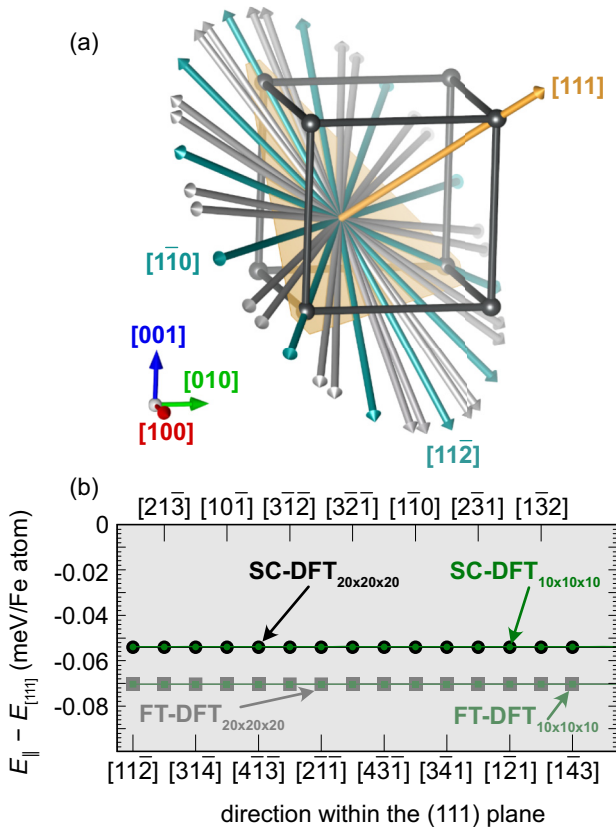


FIG. 6. Calculated uniaxial anisotropy energy within the (111) plane of BiFeO<sub>3</sub>. (a) Sketch of the pseudocubic Brillouin zone (BZ) with different lattice directions. The shaded area shows the (111) plane, whereas the anisotropy calculations have been performed considering the G-type antiferromagnet with the application of spin-orbit coupling in all directions represented by the arrows. The colored arrows in the (111) plane represent [110] and [112] and their equivalent directions. (b) Results of the calculations for part of the data. The results do not change for the complete rotation within the (111) plane. “SC-DFT” corresponds to self-consistent density functional theory calculations, and “FT-DFT” denotes calculations using the force theorem [44]. For each type of calculations, we considered different  $k$ -point sets, i.e.,  $20 \times 20 \times 20$  and  $10 \times 10 \times 10$ , in the whole BZ.

anisotropy of order 6 and of amplitude  $1.46 \mu\text{eV}$ . Such an energy is not resolvable in the energy range of Fig. 6.

#### IV. DISCUSSION

Noncollinear magnetic ground states are typically created by the interplay between the DM interaction, the exchange interaction, and the anisotropy. It has been shown [55–57] that a critical DM interaction  $D_C \propto \sqrt{JK}$  needs to be overcome to induce a noncollinear ground state such as a spin spiral. Our calculations show that the spin-current DM interaction is right at this threshold. Taking the above-determined interactions into account, the magnetic ground state is a collinear G-type AFM. Both the type-I and type-II spin cycloids propagating in the [110] and [112] directions, respectively, are degenerate in energy at  $+0.02 \text{ meV/Fe atom}$  higher in energy, which

explains why so many different spin spirals were observed in BFO [8,9,11,21,58].

Even if our calculated DFT energies have typically a precision of the order of around  $10 \mu\text{eV}$ , small deviations originating from structural relaxations, kinetic energies, and potential energies of spin spirals and from pseudocubic approximations would not affect the general conclusion.

Finally, our main results are compared with previous work. Three methods were used to determine the DM interaction in BFO.

Firstly, the magnetic interactions can be obtained from fitting experimental results from spectroscopy data, as, e.g., in Refs. [28,30,59]: In those papers, the spin-current driven DM interaction ranges from 0.1 to 0.17 meV, which is a factor of 2–3 larger than our calculated value (cf. Table I). In that case, the exchange interaction and anisotropy obtained from experiment or theory lead to a spin spiral ground state.

Secondly, the magnetic interactions can be obtained by using effective Hamiltonians and Monte Carlo simulations as in Refs. [23,25,48]: Depending on the exchange and the anisotropy energies, the parameter  $C_{ij}$  is varied to favor either the G-type AFM collinear state or the different types (type I or type II) of cycloidal directions. Our value of  $C_1 \approx 13.1 \times 10^{-6} \text{ hartrees } \mu_B^{-2} \text{ bohr}^{-1}$  is in the same energy range as these previous investigations. While, in Ref. [23], the cycloid is stable for  $C$  in between  $3 \times 10^{-6}$  and  $5 \times 10^{-6} \text{ hartrees } \mu_B^{-2} \text{ bohr}^{-1}$ , in Ref. [48] the type-I cycloid occurs for  $12 \times 10^{-6} < C < 42 \times 10^{-6} \text{ hartrees } \mu_B^{-2} \text{ bohr}^{-1}$ , and the type-II cycloid occurs for larger values. Recently, all possible cycloids have been explored by varying the ratio  $C_1 : C_2$  [25]. This work shows that both type-I and type-II cycloids can be obtained for dominant spin-current DM or Levy-Fert DM interactions. Our value lies at the boundary between the [110], [112], and [111] cycloid stability regions in accordance with the slope of the DM interaction in the directions of Fig. 4(b).

Thirdly, using the four-state method, the magnetic interactions can be obtained from DFT calculations as in Ref. [47]: In this method, the generalized exchange tensor is obtained, and the symmetry of the DM interaction is ignored. The magnetic Hamiltonian allows for a direct comparison, even though the DM interaction is determined from the LF model being  $D_1 \approx 0.126 \text{ meV}$ , about a factor of 2 larger than our value presented here.

At last, note that the same method as in this paper has been applied to study the influence of the structural distortions on the magnetic ground state in BFO [33]. In this paper, the DM interaction is determined using the LF model because only certain propagation directions of spin spirals have been calculated where the LF model coincides with the SC model. Therefore the values are close,  $D = 0.342 \text{ meV/Fe atom}$  compared with  $C_{\text{eff}} = 0.301 \text{ meV/Fe atom}$  of Table I.

Despite the differences in all the methods and their potential weaknesses in accuracy, the same order of magnitude is found for all of the presented values. Hence the overall agreement is very reasonable.

#### V. CONCLUSION

Our work demonstrates based on density functional theory that the Dzyaloshinskii-Moriya interaction in  $R3c$  bulk

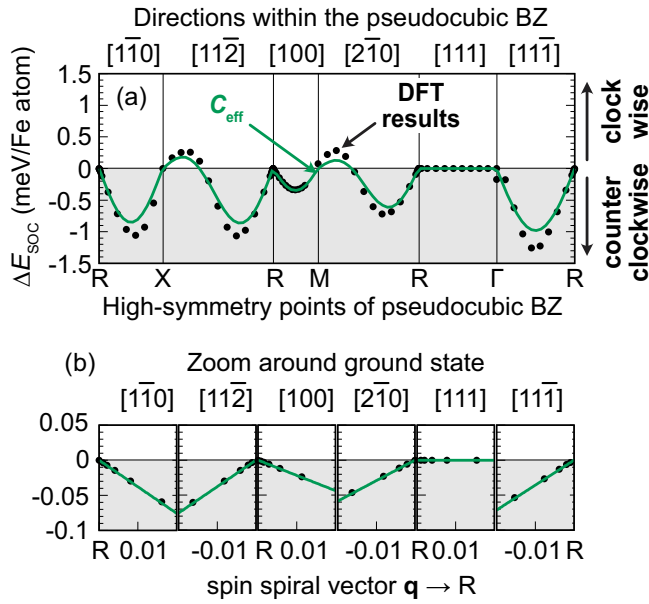


FIG. 7. Energy contribution due to spin-orbit coupling ( $\Delta E_{\text{SOC}}$ ) to the energy dispersion of spin spirals along different directions within the pseudocubic Brillouin zone [BZ; see Fig. 3(a) in the main text]. Points show calculated energies from density functional theory (DFT), and the green curve corresponds to the spin-current model in the effective nearest-neighbor approximation. Positive (negative) values prefer a clockwise (counterclockwise) sense of rotation of noncollinear states. (a) Whole calculated paths. (b) Zoom around the ground state at  $\mathbf{q} \rightarrow R$ .

BiFeO<sub>3</sub> is governed by the spin-current model stemming from the noncollinear antiferromagnetic structure. The off-centered displacement of Fe and Bi induces an asymmetric shape of the internal potential in the Fe atoms, and consequently, the Fe atoms carry almost the whole contribution to the DM interaction. This effect might not be restricted to BFO in particular and should occur in other multiferroic materials.

In the case of BFO, by including exchange interaction, DM interaction, and anisotropy, we show that any spin cycloid propagation direction in the (111) plane is energetically degenerate. This could explain an effect of continuously rotating cycloids in BFO that has recently been observed [58] and explained as a surface effect. Based on our results, this effect should also be measurable in the bulk.

## ACKNOWLEDGMENTS

S.M. and B.D. thank Dr. Manuel Bibes and Dr. Eric Bousquet for fruitful discussions and careful reading of the manuscript. This work is supported by the National Natural Science Foundation of China under Grant No. 12074277, the startup fund from Soochow University, and Priority Academic Program Development (PAPD) of Jiangsu Higher Education Institutions. S.M., M.J.V., B.D., and L.B. acknowledge DARPA Grant No. HR0011727183-D18AP00010 (TEE Program) and the European Union's Horizon 2020 research and innovation program under Grant Agreement No. 964931 (TSAR). L.B. also thanks the ARO for Grant No. W911NF-21-1-0113 and the Vannevar Bush Faculty Fellowship (VBFF) Grant No. N00014-20-1-2834 from the Department of Defense. Computing time was provided by ARCHER and ARCHER2 based in the United Kingdom at the National Supercomputing Service with support from PRACE aishl and from the Consortium d'Equipements de Calcul Intensif (FRS-FNRS Belgium GA 2.5020.11).

## APPENDIX: EFFECTIVE DM INTERACTION FROM SPIN-CURRENT MODEL

As stated in the main text, using an effective nearest-neighbor approximation for the spin-current driven Dzyaloshinskii-Moriya interaction leads to a very good description of the calculated data. In Fig. 7 the green curve shows the result with an effective spin-current DM interaction,  $C_{\text{eff}} \approx C_{ij}(\mathbf{q} \rightarrow R)$  of +0.301 meV/Fe atom, also presented in Table I.

- [1] Y. E. Roginskaya, Y. Y. Tomashpol'skiĭ, Y. N. Venevtsev, V. M. Petrov, and G. S. Zhdanov, *Sov. Phys. JETP* **23**, 47 (1966).
- [2] J. B. Neaton, C. Ederer, U. V. Waghmare, N. A. Spaldin, and K. M. Rabe, *Phys. Rev. B* **71**, 014113 (2005).
- [3] I. A. Kornev, S. Lisenkov, R. Haumont, B. Dkhil, and L. Bellaiche, *Phys. Rev. Lett.* **99**, 227602 (2007).
- [4] R. Haumont, I. A. Kornev, S. Lisenkov, L. Bellaiche, J. Kreisel, and B. Dkhil, *Phys. Rev. B* **78**, 134108 (2008).
- [5] P. Ravindran, R. Vidya, A. Kjekshus, H. Fjellvåg, and O. Eriksson, *Phys. Rev. B* **74**, 224412 (2006).
- [6] I. Dzyaloshinsky, *J. Phys. Chem. Solids* **4**, 241 (1958).
- [7] T. Moriya, *Phys. Rev.* **120**, 91 (1960).
- [8] I. Sosnowska, T. P. Neumaier, and E. Steichele, *J. Phys. C: Solid State Phys.* **15**, 4835 (1982).
- [9] I. Sosnowska, R. Przeniosło, P. Fischer, and V. Murashov, *J. Magn. Magn. Mater.* **160**, 384 (1996).
- [10] W. Ratcliff, D. Kan, W. Chen, S. Watson, S. Chi, R. Erwin, G. J. McIntyre, S. C. Capelli, and I. Takeuchi, *Adv. Funct. Mater.* **21**, 1567 (2011).
- [11] D. Sando, A. Agbelele, D. Rahmedov, J. Liu, P. Rovillain, C. Toulouse, I. C. Infante, A. P. Pyatakov, S. Fusil, E. Jacquet, C. Carrétéro, C. Deranlot, S. Lisenkov, D. Wang, J.-M. Le Breton, M. Cazayous, A. Sacuto, J. Juraszek, A. K. Zvezdin, L. Bellaiche *et al.*, *Nat. Mater.* **12**, 641 (2013).
- [12] J. Bertinshaw, R. Maran, S. J. Callori, V. Ramesh, J. Cheung, S. A. Danilkin, W. T. Lee, S. Hu, J. Seidel, N. Valanoor, and C. Ulrich, *Nat. Commun.* **7**, 12664 (2016).
- [13] S. R. Burns, D. Sando, B. Xu, B. Dupé, L. Russell, G. Deng, R. Clements, O. H. Paull, J. Seidel, L. Bellaiche, N. Valanoor, and C. Ulrich, *npj Quantum Mater.* **4**, 18 (2019).
- [14] A. Haykal, J. Fischer, W. Akhtar, J.-Y. Chauleau, D. Sando, A. Finco, F. Godel, Y. A. Birkhölzer, C. Carrétéro, N. Jaouen, M. Bibes, M. Viret, S. Fusil, V. Jacques, and V. Garcia, *Nat. Commun.* **11**, 1704 (2020).
- [15] L. W. Martin, S. P. Crane, Y.-H. Chu, M. B. Holcomb, M. Gajek, M. Huijben, C.-H. Yang, N. Balke, and R. Ramesh, *J. Phys.: Condens. Matter* **20**, 434220 (2008).

- [16] C. Thiele, K. Dörr, O. Bilani, J. Rödel, and L. Schultz, *Phys. Rev. B* **75**, 054408 (2007).
- [17] J. M. Rondinelli, M. Stengel, and N. A. Spaldin, *Nat. Nanotechnol.* **3**, 46 (2008).
- [18] P. Rovillain, R. de Sousa, Y. Gallais, A. Sacuto, M. A. Méasson, D. Colson, A. Forget, M. Bibes, A. Barthélémy, and M. Cazayous, *Nat. Mater.* **9**, 975 (2010).
- [19] S. Manipatruni, D. E. Nikonov, C.-C. Lin, T. A. Gosavi, H. Liu, B. Prasad, Y.-L. Huang, E. Bonturim, R. Ramesh, and I. A. Young, *Nature (London)* **565**, 35 (2019).
- [20] E. Parsonnet, L. Caretta, V. Nagarajan, H. Zhang, H. Taghinejad, P. Behera, X. Huang, P. Kavle, A. Fernandez, D. Nikonov, H. Li, I. Young, J. Analytis, and R. Ramesh, *Phys. Rev. Lett.* **129**, 087601 (2022).
- [21] I. Sosnowska and A. K. Zvezdin, *J. Magn. Magn. Mater.* **140**, 167 (1995).
- [22] H. Katsura, N. Nagaosa, and A. V. Balatsky, *Phys. Rev. Lett.* **95**, 057205 (2005).
- [23] D. Rahmedov, D. Wang, J. Íñiguez, and L. Bellaiche, *Phys. Rev. Lett.* **109**, 037207 (2012).
- [24] C. Ederer and N. A. Spaldin, *Phys. Rev. B* **71**, 060401(R) (2005).
- [25] B. Xu, B. Dupé, C. Xu, H. Xiang, and L. Bellaiche, *Phys. Rev. B* **98**, 184420 (2018).
- [26] C. Weingart, N. Spaldin, and E. Bousquet, *Phys. Rev. B* **86**, 094413 (2012).
- [27] H. Dixit, J. H. Lee, J. T. Krogel, S. Okamoto, and V. R. Cooper, *Sci. Rep.* **5**, 12969 (2015).
- [28] M. Matsuda, R. S. Fishman, T. Hong, C. H. Lee, T. Ushiyama, Y. Yanagisawa, Y. Tomioka, and T. Ito, *Phys. Rev. Lett.* **109**, 067205 (2012).
- [29] R. S. Fishman, J. T. Haraldsen, N. Furukawa, and S. Miyahara, *Phys. Rev. B* **87**, 134416 (2013).
- [30] U. Nagel, R. S. Fishman, T. Katuwal, H. Engelkamp, D. Talbayev, H. T. Yi, S.-W. Cheong, and T. Room, *Phys. Rev. Lett.* **110**, 257201 (2013).
- [31] R. Fishman, *Phys. B (Amsterdam)* **536**, 115 (2018).
- [32] A. Fert and P. M. Levy, *Phys. Rev. Lett.* **44**, 1538 (1980).
- [33] B. Xu, S. Meyer, M. J. Verstraete, L. Bellaiche, and B. Dupé, *Phys. Rev. B* **103**, 214423 (2021).
- [34] X. Gonze, B. Amadon, P. M. Anglade, J. M. Beuken, F. Bottin, P. Boulanger, F. Bruneval, D. Caliste, R. Caracas, M. Côté, T. Deutsch, L. Genovese, Ph. Ghosez, M. Giantomassi, S. Goedecker, D. R. Hamann, P. Hermet, F. Jollet, G. Jomard, S. Leroux *et al.*, *Comput. Phys. Commun.* **180**, 2582 (2009).
- [35] X. Gonze, F. Jollet, F. A. Araujo, D. Adams, B. Amadon, T. Applencourt, C. Audouze, J.-M. Beuken, J. Bieder, A. Bokhanchuk, E. Bousquet, F. Bruneval, D. Caliste, M. Côté, F. Dahm, F. Da Pieve, M. Delaveau, M. Di Gennaro, B. Dorado, C. Espejo *et al.*, *Comput. Phys. Commun.* **205**, 106 (2016).
- [36] X. Gonze, B. Amadon, G. Antonius, F. Arnardi, L. Baguet, J.-M. Beuken, J. Bieder, F. Bottin, J. Bouchet, E. Bousquet, N. Brouwer, F. Bruneval, G. Brunin, T. Cavignac, J.-B. Charraud, W. Chen, M. Côté, S. Cottenier, J. Denier, G. Geneste *et al.*, *Comput. Phys. Commun.* **248**, 107042 (2020).
- [37] P. E. Blöchl, *Phys. Rev. B* **50**, 17953 (1994).
- [38] H. Krakauer, M. Posternak, and A. J. Freeman, *Phys. Rev. B* **19**, 1706 (1979).
- [39] E. Wimmer, H. Krakauer, M. Weinert, and A. J. Freeman, *Phys. Rev. B* **24**, 864 (1981).
- [40] M. Weinert, E. Wimmer, and A. J. Freeman, *Phys. Rev. B* **26**, 4571 (1982).
- [41] <https://www.flapw.de/MaX-6.0/>.
- [42] S. H. Vosko, L. Wilk, and M. Nusair, *Can. J. Phys.* **58**, 1200 (1980).
- [43] L. M. Sandratskii, *J. Phys.: Condens. Matter* **3**, 8565 (1991).
- [44] A. Mackintosh and O. Andersen, in *Electrons at the Fermi Surface*, edited by M. Springford (Cambridge University Press, London, 1980), pp. 149–224.
- [45] A. Oswald, R. Zeller, P. J. Braspenning, and P. H. Dederichs, *J. Phys. F: Met. Phys.* **15**, 193 (1985).
- [46] M. Heide, G. Bihlmayer, and S. Blügel, *Phys. B (Amsterdam)* **404**, 2678 (2009).
- [47] C. Xu, B. Xu, B. Dupé, and L. Bellaiche, *Phys. Rev. B* **99**, 104420 (2019).
- [48] S. Bhattacharjee, D. Rahmedov, L. Bellaiche, and D. Wang, *MRS Commun.* **3**, 213 (2013).
- [49] P. M. Levy and A. Fert, *C. R. Phys.* **17**, 447 (2016).
- [50] Note that in the data without SOC, we see a tiny energy difference between the perfectly collinear state (*R* points) and the next states. This energy difference stems from the rotation of magnetization as it is implemented in the FLAPW method.
- [51] B. Dupé, G. Bihlmayer, M. Böttcher, S. Blügel, and S. Heinze, *Nat. Commun.* **7**, 11779 (2016).
- [52] Note that SOC calculations with first-order perturbation have shown consistent results with self-consistent ones, as shown in Refs. [60,61].
- [53] L. Desplat, S. Meyer, J. Bouaziz, P. M. Buhl, S. Lounis, B. Dupé, and P.-A. Hervieux, *Phys. Rev. B* **104**, L060409 (2021).
- [54] H. Yang, G. Chen, A. A. C. Cotta, A. T. N'Diaye, S. A. Nikolaev, E. A. Soares, W. A. A. Macedo, K. Liu, A. K. Schmid, A. Fert, and M. Chshiev, *Nat. Mater.* **17**, 605 (2018).
- [55] A. Bocdanov and A. Hubert, *Phys. Status Solidi B* **186**, 527 (1994).
- [56] U. K. Rößler, A. N. Bogdanov, and C. Pfleiderer, *Nature (London)* **442**, 797 (2006).
- [57] S. Rohart and A. Thiaville, *Phys. Rev. B* **88**, 184422 (2013).
- [58] A. Finco, A. Haykal, S. Fusil, P. Kumar, P. Dufour, A. Forget, D. Colson, J.-Y. Chaudreau, M. Viret, N. Jaouen, V. Garcia, and V. Jacques, *Phys. Rev. Lett.* **128**, 187201 (2022).
- [59] R. S. Fishman, N. Furukawa, J. T. Haraldsen, M. Matsuda, and S. Miyahara, *Phys. Rev. B* **86**, 220402(R) (2012).
- [60] S. Meyer, B. Dupé, P. Ferriani, and S. Heinze, *Phys. Rev. B* **96**, 094408 (2017).
- [61] B. Zimmermann, G. Bihlmayer, M. Böttcher, M. Bouhassoune, S. Lounis, J. Sinova, S. Heinze, S. Blügel, and B. Dupé, *Phys. Rev. B* **99**, 214426 (2019).